water

MDPI

Article

Development of Biochars Derived from Water Bamboo (*Zizania latifolia*) Shoot Husks Using Pyrolysis and Ultrasound-Assisted Pyrolysis for the Treatment of Reactive Black 5 (RB5) in Wastewater

Thanh Tam Nguyen [1,2,3], Hung-Hsiang Chen [3], Thi Hien To [1,2], Yu-Chen Chang [3], Cheng-Kuo Tsai [4], Ku-Fan Chen [3,*] and Yung-Pin Tsai [3,*]

[1] Department of Environmental Engineering, Faculty of Environment, University of Science (VNUHCM), Ho Chi Minh City 700000, Vietnam; ngttam@hcmus.edu.vn (T.T.N.); tohien@hcmus.edu.vn (T.H.T.)
[2] Vietnam National University Ho Chi Minh City, Ho Chi Minh City 700000, Vietnam
[3] Department of Civil Engineering, College of Science and Technology, National Chi Nan University, Puli, Nantou 545301, Taiwan; s109322901@mail1.ncnu.edu.tw (H.-H.C.); yu.chen73108@gmail.com (Y.-C.C.)
[4] Department of Safety Health and Environment, National Yunlin University of Science and Technology, Yunlin 640301, Taiwan; CKTsai@yuntech.edu.tw
* Correspondence: kfchen@ncnu.edu.tw (K.-F.C.); yptsai@ncnu.edu.tw (Y.-P.T.)

check for updates

Citation: Nguyen, T.T.; Chen, H.-H.; To, T.H.; Chang, Y.-C.; Tsai, C.-K.; Chen, K.-F.; Tsai, Y.-P. Development of Biochars Derived from Water Bamboo (*Zizania latifolia*) Shoot Husks Using Pyrolysis and Ultrasound-Assisted Pyrolysis for the Treatment of Reactive Black 5 (RB5) in Wastewater. *Water* **2021**, *13*, 1615. http://doi.org/10.3390/w13121615

Academic Editor: María Ángeles Martín-Lara

Received: 21 April 2021
Accepted: 3 June 2021
Published: 8 June 2021

Abstract: Adsorbent made by carbonization of biomass under oxygen-limited conditions has become a promising material for wastewater treatment owing to its cost-effective, simple, and eco-friendly processing method. Ultrasound is considered a green technique to modify carbon materials because it uses water as the solvent. In this study, a comparison of Reactive Black 5 (RB5) adsorption capacity between biochar (BC) generated by pyrolysis of water bamboo (*Zizania latifolia*) husks at 600 °C and ultrasound-assisted biochar (UBC) produced by pyrolysis at 600 °C assisted by ultrasonic irradiation was performed. UBC showed a greater reaction rate and reached about 80% removal efficiency after 4 h, while it took 24 h for BC to reach that level. Scanning electron microscope (SEM) images indicated that the UBC morphology surface was more porous, with the structure of the combination of denser mesopores enhancing physiochemical properties of UBC. By Brunauer, Emmett, and Teller (BET), the specific surface areas of adsorbent materials were analyzed, and the surface areas of BC and UBC were 56.296 m^2/g and 141.213 m^2/g, respectively. Moreover, the pore volume of UBC was 0.039 cm^3/g, which was higher than that of BC at 0.013 cm^3/g. The adsorption isotherms and kinetics revealed the better fits of reactions to Langmuir isotherm and pseudo-second-order kinetic model, indicating the inclination towards monolayer adsorption and chemisorption of RB5 on water bamboo husk-based UBC.

Keywords: biochar; pyrolysis; ultrasonic cavitation; water bamboo; Reactive Black 5

1. Introduction

Biochar, which is produced by thermal decomposition of carbon-rich biomass wastes under oxygen-limited conditions (<900 °C), has attracted progressive interest as a greatly promising and economical material for a number of applications, including soil amendment [1–3], carbon sequestration [4–9], activator and catalyst [10–12], electrode materials [13–16], and wastewater treatment [17–19]. This is attributed to its high carbon content, stable structure, large area, and porous surface, cation exchange capacity, and eco-friendly characteristics [20]. Biochar is a potential and low-cost adsorbent for organic and inorganic contaminants in the environment; however, the removal efficiency is lower than that of activated carbon [21]. Therefore, biochar has been modified to enhance its physiochemical properties by physical and chemical approaches [22]. To chemically modulate the properties of biochar, acid-base, oxidizing agent, and carbonaceous materials, modifications

have been applied. On the other hand, steam and gas purging are the main methods for physical modification.

However, these modifications might suffer from high costs, complex processes, potential pollution, and high energy consumption [23,24] The ultrasonic method, a green technology that requires no additional chemicals and generates no harmful products, has been recently employed as an efficient method for the activation of biochar due to the cost-effective, simple, and safe operation [24]. When ultrasound waves propagate in water, fine bubbles originating from bubble nuclei appear, grow to the resonance size, and then rapidly collapse. During the bubble collapse, extremely high temperature and pressure of 5000 K and 1000 atm are reached, respectively. Simultaneously, generated shock waves, shearing stress, and jet flow lead to the physical and chemical effects of ultrasound. At the hot spots, large particles are split into smaller ones, the material surface is smoothly cleaned, new pores are created, and the porosity of the surface increases. Consequently, biochar is structurally modified with a combination of micro and mesoporous surfaces, promoting the efficiency of technical applications, especially in the adsorption process [25].

Ultrasonic sonication-combined amination has been used to activate pinewood-derived biochar for CO_2 capture [20]. Low-frequency ultrasonic irradiation at 30 s led to the physical activation of biochar owing to the exfoliating surface and dispatching the irregular graphitic layers of biochar, creating new pores and unclogging blocked micropores. Thereafter, the porosity and permeability of biochar were enhanced, leading to more efficient functionalization and CO_2 capture. Research on camphor leaves-derived biochar synthesized by ultrasound-assisted alkali activation expressed the larger surface area and pore volume of biochar because these activations escalated surface cracks. Furthermore, ultrasonic irradiation intensified chemical etching of the biochar surface by facilitating mass transfer of molecules and particles and promoting nucleation, growth, and violent collapse of cavitation bubbles. Additionally, Pb(II) adsorption experiments were performed, and the data demonstrated the higher rapid sorption capacity of the sono-modified biochar as exhibited in the increase of sorption rate from 0.0005 to 0.0208 (40 times) compared to raw biochar with pyrolysis [23]. In 2019, ultrasonic pretreatment of switchgrass and miscanthus biochar in the presence of CO_2 within a short irradiation time led to a significant increase of heating value of biochar gasification, which reduced the energy consumption and processing time of biochar preparation [26].

Because of their peculiar advantages, like bright colors, ease of application, brilliant shades, and excellent colorfastness, reactive dyes have been increasingly used in the textile industry, especially Reactive Black 5 (RB5), contributing to 50% of the reactive dyes worldwide [27,28]. However, discharge of RB5, with poor biodegradability and high solubility, into the environment threatens the ecosystem and health because RB5 and its intermediates are highly toxic, causing carcinogenic, mutagenic, and allergic effects. Moreover, they can also reduce the sunlight penetration into water, which affects aquatic creatures. The elimination of reactive dyes from wastewater by conventional physicochemical and biological treatment methods is difficult because of their highly soluble properties [29].

The adsorption process has been found to be one of the superior pathways to treat RB5 due to its low cost, simplicity, and efficiency [30]. There have been a variety of biomass successfully applied in the production of biochar for RB5 removal, including walnut [31], carob [32], and bamboo [27]. Water bamboo (*Zizania latifolia*) shoot is one of the major agricultural products in Puli Township, Nantou County, Taiwan; therefore, the water bamboo husk waste is readily available, free of charge, and is an eco-friendly source to reuse in the adsorption application [33].

Water bamboo husk is carbon-rich agricultural waste that has the potential to develop biochar for the removal of water pollutants. Additionally, ultrasound is a practical technique to increase pores and enhance the pollutant removal ability of biochar. In this study, the outer husks of water bamboo shoots were used to prepare biochar (BC) for RB5 removal by pyrolysis. Simultaneously, ultrasound-assisted biochar (UBC) was produced by pyrolysis and accompanied by ultrasonic irradiation. This work was aimed at creating a

new biochar material from water bamboo husks with enhanced physicochemical properties by low energy-consuming ultrasonic irradiation for RB5 removal in the wastewater. The equilibrium isotherms and adsorption kinetics were studied to perceive the adsorption mechanisms of RB5 molecules onto the produced water bamboo-derived UBC.

2. Materials and Methods

2.1. Materials and Analytical Methods

The adsorbate, RB5, was imported from Sigma-Aldrich, MO, USA. The dye solution was prepared with deionized (DI) water, and 0.1 M HCl or NaOH was used to adjust the pH. The chemical formula of RB5 (4-amino-5-hydroxy-3,6-bis ((4-((2-sulfooxy)ethyl)sulfonyl)phenyl)azo)-2,7-naphthalenedisulfonic acid tetrasodium salt) is $C_{26}H_{21}N_5Na_4O_{19}S_6$, and RB5 molecular weight is 991.82 g/mol. The structural formula of RB5 is shown in Figure S1. RB5 is an anionic dye because, after dissolution, anionic sulfonate exists in the solution [34]. The RB5 concentration was measured by DR 5000 UV-Vis spectrophotometer (HACH, CO, USA). A wavelength of 597 nm was used for all measurements because the RB5 absorption peaks were the same at the value of 597 nm at all different pH values (Figure S2). All samples gathered from the adsorption tests were filtered through a 0.45-μm filter membrane prior to examination to eliminate carbon fines.

2.2. BC and UBC Preparation and RB5 Adsorption-Capacity Comparison

Water bamboo husks were collected from Puli Township, Nantou County, Taiwan. The husks were then washed with water, cut into small pieces (about 2–3 cm), and dried in an oven at 105 °C for several days. Chopped water bamboo husks were ground by a grinder and sieved with a 2 mm screen. Thereafter, the powder was placed into a muffle furnace (Chengsang, Taiwan) and carbonized at 600 °C for 2 h with the heating rate of 5 °C/min and the nitrogen flow rate of 1 L/min. After carbonization, the powder was cooled and washed several times with DI water until the washing water became neutral. Finally, the BC was oven-dried at 105 °C for 2 days and then stored in a glass bottle.

UBC was prepared from water bamboo biochar assisted by ultrasonic irradiation. Air-saturated DI water was employed in all tests, and a water bath was employed to maintain the water temperature at 25 °C. Then, 0.5 g BC was added into 25 mL air-saturated water and left at rest in a bottle for 30 min before sonicating. After being irradiated, the water in UBC was removed by a vacuum filtration pump. UBC was dried in an oven at 105 °C overnight, followed by cooling down to room temperature, and stored in a glass bottle. To produce UBC, an ultrasonic sonicator (130PB, Sonics & Materials Inc., CT, USA) was used at an ultrasonic frequency of 20 kHz and the electric power of 65 W. Different irradiation times were applied to study the optimal physicochemical properties of UBC as well as the RB5 adsorption capacity.

Different irradiation times at 0, 0.5, 1, 3, 5, and 8 min were applied to assess the impact of irradiation time on UBC characteristics. To compare the RB5 removal efficiency between BC and UBC, the experiments were carried out at RB5 initial concentration of 10 mg/L and adsorbent dosage of 10 g/L for 8 h.

To compare the RB5 adsorption capacity of BC and UBC, adsorption experiments were conducted by adding 10 g/L BC or UBC to 10 mL RB5 at a concentration of 10 mg/L. The glass bottles were sealed and put in an orbital shaking incubator (Kansin Instruments Co., LTD., Taiwan) with a shaking speed of 150 rpm. Afterward, a UV-Vis spectrophotometer's remaining concentration of RB5 was measured at 597 nm after filtering by a 0.45-μm filter membrane.

2.3. Characterization of BC and UBC

Brunauer, Emmett, and Teller (BET) were applied to investigate the specific surface area using adsorption data in the relative pressure range from 0.05 to 0.30. (AutoSorb iQ-TPX, Quantachrome Instruments, FL, USA), and the Barrett–Joyner–Halenda (BJH) method was utilized to calculate the pore volume. The surface morphology was obtained by scan-

ning electron microscopy (SEM, JSM-7800F, JEOL, Japan). The surface functional groups were determined by Fourier transform infrared (FTIR) spectroscopy (Spectrum one, Perkin-Elmer, CT, USA) in the range 2000–500 cm^{-1}. Zeta potential and isoelectric point were measured at pH 2 to 12 by a zeta potential meter (Zeta-Meter 4.0, Shin Shiang, Taiwan).

2.4. Adsorption Equilibrium Isotherm Experiments

The impact of various experimental conditions on the RB5 removal performance of prepared UBC was investigated, including adsorbent dosage, solution pH, RB5 initial concentration, and reaction time. Experimental conditions were 10 mL RB5 (10–100 mg/L), UBC dosage (1–30 g/L), pH (2–12), and contact time (0.5–96 h). All the experiments were conducted at 25 °C with the exception of adsorption kinetics studies. Experiments were carried out at 15, 25, and 35 °C to study adsorption kinetics. Triplicate tests were implemented for each experiment.

The RB5 removal efficiency, H (%), and adsorption capacity $\left(q_{e(exp)},\ \text{mg g}^{-1}\right)$ were calculated by the following equations:

$$H = \frac{C_0 - C_t}{C_0} \times 100 \tag{1}$$

$$q_{e(exp)} = \frac{C_0 - C_e}{m} \times V \tag{2}$$

where C_0 and C_t define the RB5 concentration at time t = 0 and t; C_e is the equilibrium concentration of UBC (mg/L); V (L) is the volume of RB5; and m (g) is the mass of UBC.

The Langmuir and Freundlich models were utilized to investigate isotherm parameters using Equations (3) and (4), respectively [35,36].

$$\frac{q_e}{q_m} = \frac{bC_e}{1 + bC_e} \tag{3}$$

$$q_e = K_f \cdot {C_e}^{1/\boldsymbol{n}} \tag{4}$$

where q_e (mg/g) is the equilibrium adsorption capacity; q_m (mg/g) is the maximum monolayer adsorption capacity; b (L/mg) is the Langmuir constant, which relates to the binding energy; C_e is the equilibrium concentration of the adsorbate (mg/L); K_f $(\text{mg/g}(\text{L/mg})^{1/n})$; and $\boldsymbol{n}$ are the Freundlich constants.

2.5. Adsorption Kinetics Studies

The experimental kinetic data is illustrated in the pseudo-first-order kinetic and pseudo-second-order kinetic models utilizing the following equations to assess the reaction rate and mechanisms of RB5 adsorption on UBC [37]. Kinetic tests were performed using UBC dosage, pH, and RB5 initial concentration obtained from previous experiments at 15, 25, and 35 °C for 96 h.

$$\log(q_e - q_t) = \log q_e - \frac{k_1}{2.303} t \tag{5}$$

$$\frac{t}{q_t} = \frac{1}{k_2 q_e^2} + \frac{1}{q_e} t \tag{6}$$

where q_e and q_t (mg/g) denote adsorption capacities at equilibrium and time t (h), respectively, k_1 (h^{-1}) is the adsorption rate constant, and k_2 is the rate regular of pseudo-second-order adsorption kinetics.

3. Results and Discussion

3.1. Effect of Ultrasonic Irradiation Time on UBC Properties

The chemical and mechanical effect of acoustic cavitation strongly depends on the ultrasonic frequency [38]. The cavitating bubbles are larger at low frequency, and their collapses were more violent due to the higher jet velocity. It is also known that the physical

effect of acoustic cavitation promoted from shock waves, shearing stress, and jet flow, which is favored at low frequency, enables the surface morphology and structure modifying of BC [39,40]. Therefore, an ultrasonic frequency of 20 kHz was used in this study to activate water bamboo-based BC.

Figure 1 illustrates that the removal efficiency of RB5 was enhanced by the carbon modified by ultrasonic irradiation. RB5 removal efficiency of UBC depended on irradiation time and reached the highest value at 3 min. Upon increased irradiation time, RB5 removal efficiency declined again. This can be ascribed to the intense acoustic cavitation in the solution, which destroyed the UBC structure and pores. Therefore, an ultrasonic irradiation time of 3 min was used for all subsequent experiments.

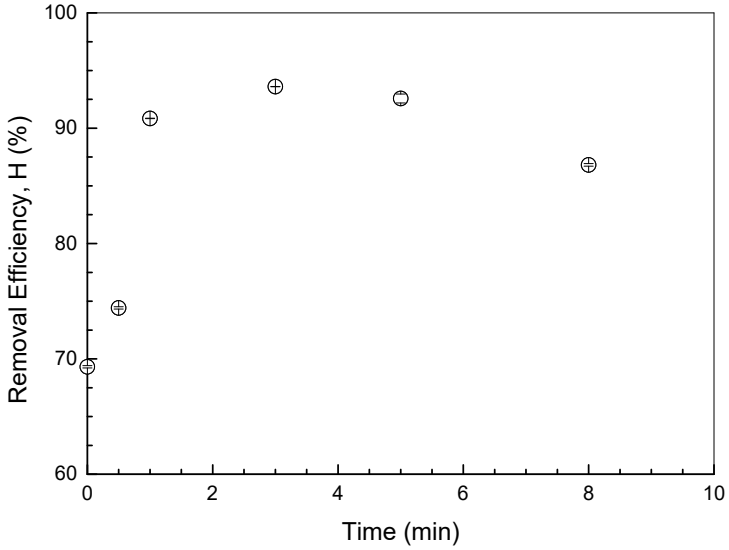

Figure 1. Dependence of RB5 removal efficiency on irradiation time.

3.2. Comparison of RB5 Adsorption Capacity by BC and UBC

Figure 2 exhibits the RB5 removal efficiency and adsorption capacity of BC and UBC up to 48 h. The removal efficiency and adsorption capacity of UBC were comparatively higher than that of BC throughout the whole experimental duration. At 0.5 h, the removal efficiency of RB5 was 51.14% for UBC and 36.53% for BC, and it reached to about 80% after 4 h and 24 h for UBC and BC, respectively, indicating that UBC performed the higher reaction rate. The highest RB5 removal efficiency was 89.95% and 83.10% for UBC and BC, respectively. It can be elucidated by the difference of surface morphology of UBC and BC. In other words, cavitation might open new micropores and mesopores; subsequently, surface morphology was modified, and physicochemical properties were improved.

Figure 3 shows FTIR spectra of RB5, BC, UBC, and UBC absorbed RB5. As compared FTIR spectra of BC and UBC in Figure 3, there was no new peak of functional groups, indicating that UBC was only physically modified by ultrasonic irradiation at 20 kHz due to surface excoriation [24]. However, there were discrepancies on the spectra of UBC and UBC adsorbed RB5. The peak of C=C group appeared at 875 cm^{-1}, which was in accordance with spectrum of RB5. Besides, the peaks of C-O secondary alcohol stretch were observed at 1132 cm^{-1} and 1107 cm^{-1} on the spectra of RB5- and UBC-adsorbed RB5, respectively, demonstrating the adsorption of RB5 on UBC. Since the amount of RB5 adsorbed onto UBC was small compared to the dosage of UBC, other functional groups of RB5 on UBC shown in FTIR may not be significant.

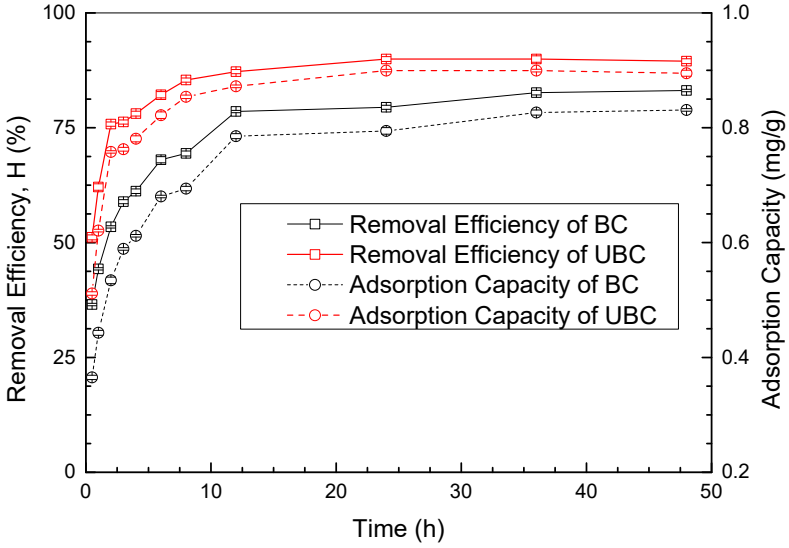

Figure 2. Comparison of RB5 removal efficiency and adsorption capacity between BC and UBC.

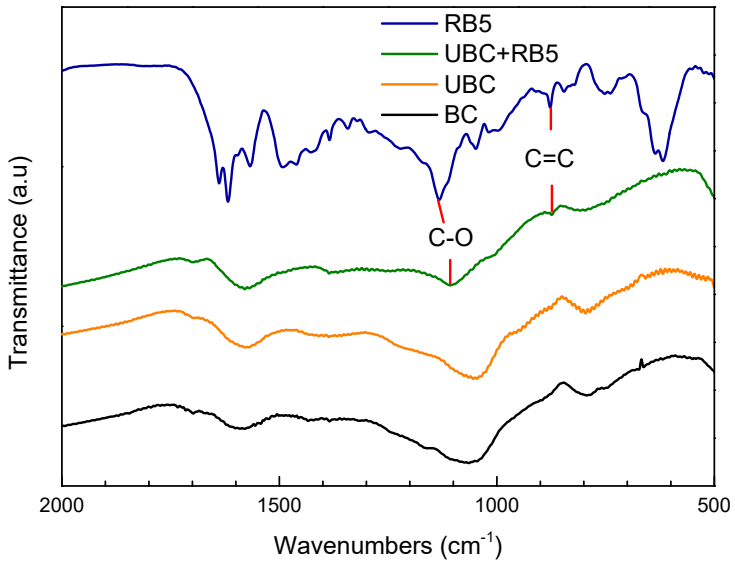

Figure 3. FTIR spectra of RB5, BC, UBC, and UBC absorbed RB5.

As can be seen from Figure 4, in the SEM images of BC and UBC, dense mesopores with diameters between 2 and 50 nm are exposed on the UBC surface (Figure 4b), possibly leading to the greater rate of RB5 removal. It was reported that the molecular size of RB5 (2.990 nm × 0.875 nm) [41] was slightly greater than micropores (<2 nm); therefore, it seemed unable for unopened pores and micropores of BC to capture RB5. The BET surface areas were 141.213 and 56.296 m^2/g for UBC and BC, respectively. The pore volume of UBC and BC were 0.039 and 0.013 cm^3/g, respectively. Therefore, the enhancement in the surface area and porosity of UBC, which was produced by an ultrasonic-assisted process, fostered the adsorption capacity of UBC due to shockwaves and microjets with the high velocity generated from the bubble collapse. In Chatterjee R et al. [25], the surface of raw pinewood-derived biochar was rough and contained blocked pores, whereas the surface of ultrasound-activated biochar was more porous and consisted of numerous opened pores. There were pores on the layer adjacent to the surface and interlayers because of the aid of ultrasound-penetrating under-layers in breaking biochar structure and creating additional pores. It was also reported that the surface properties of biochar were enhanced by ultrasonic power assisting slow pyrolysis without changing the chemical characteristics.

Thermal gravimetric analysis displayed that, with ultrasonic pre-treatment, the thermal stability of samples was higher than that of untreated samples, indicating the pre-treated biochar was more structurally stable. The material surface became cleaner, contained more micropores, and microchannels appeared, as seen in SEM images. The surface area slightly increased from 10.48 to 12.40 m^2/g. Besides, pre-treated samples also proved to have a larger Cu(II)-sorption capacity [42]. Experimental data of this research also demonstrated that ultrasound-assisted modification was effective to improve the surface properties of water bamboo-based biochar and its performance for the removal of the pollutant.

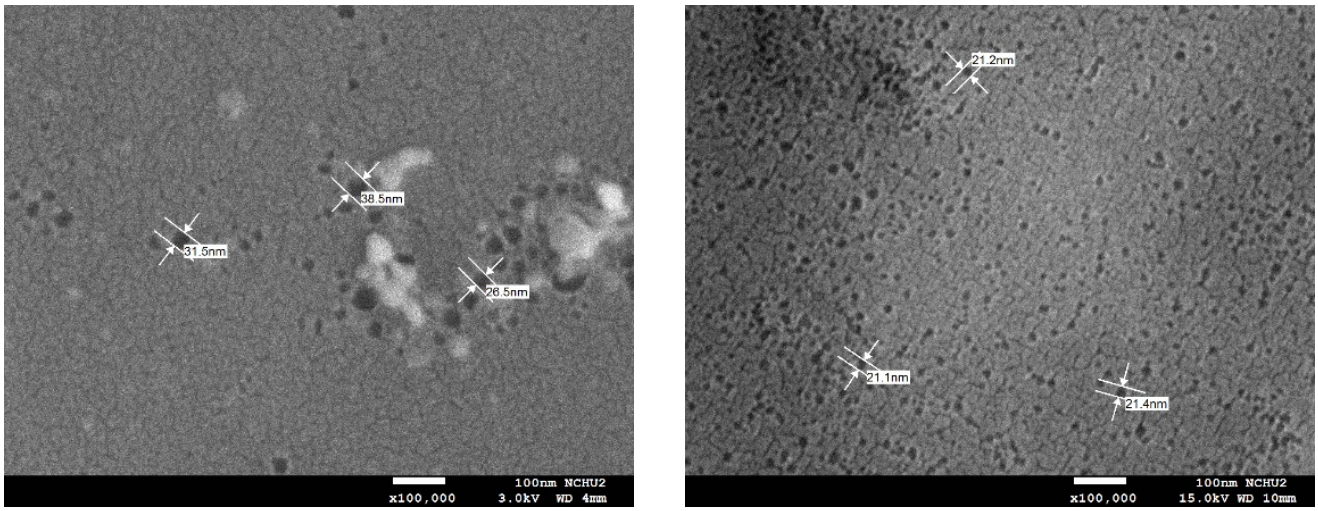

Figure 4. SEM images of (**a**) BC and (**b**) UBC.

The results showed that UBC had larger RB5-removal efficiency, specific surface area, pore volume, and amount of mesopores than BC. Therefore, in the next part of the study, the experiments focused on optimizing the operating parameters and evaluating the adsorption mechanisms by adsorption isotherms and kinetics of UBC, since UBC is more applicable than BC for the treatment of RB5.

3.3. Effects of Operating Conditions on RB5 Adsorption of UBC

3.3.1. UBC Dosage

This batch experiment was conducted at the initial RB5 solution pH (pH 6) with a concentration of 10 mg/L and a volume of 10 mL for 3 h. The UBC dosages were applied in the range of 1 to 30 g/L. As shown in Figure 5, the removal efficiency enhanced, firstly, with the increase in UBC dosage and became unstable from 12 g/L. The adsorption capacity increased sharply from 1 to 3 g/L, then slightly increased until 5 g/L with the adsorption capacity of about 0.80 mg/g, and was followed by a decrease from 8 g/L, as seen in Figure 5. With higher UBC doses, increasing the surface area and the adsorption site led to a higher adsorption rate [43,44]. This could be the explanation for the augmentation of adsorption capacity as the absorbent quantity increased. However, a further increase in the UBC dosage from 10 g/L speedily reduced the RB5-adsorption capacity. There might be a conglomeration and interaction of adsorbent particles, which resulted from a high adsorbent amount leading to the decrement of adsorption capacity [45,46]. Consequently, the total surface area reduced, the diffusional path length increased, and hence the functional groups, through adsorption processes, became unsaturated [47,48]. Based on the good RB5 removal efficiency and high adsorption capacity, the UBC dosage of 10 g/L was fixed for the following experiments.

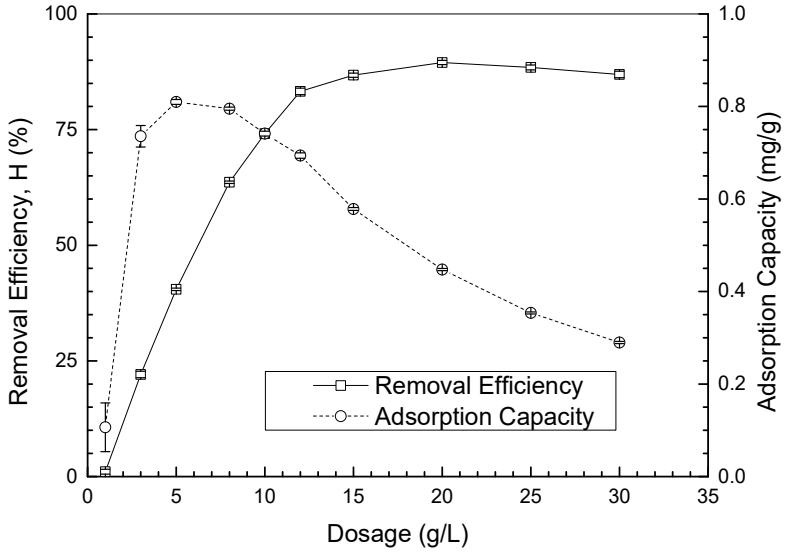

Figure 5. Impact of UBC dosage on adsorption of RB5 on UBC.

3.3.2. Solution pH

In Figure 6, RB5 removal efficiency and capacity are plotted against the solution pH, which describes the strong influence of pH on RB5 adsorption of UBC. The RB5 removal efficiency was greatest at pH 2, and nearly all of the total RB5 was removed. The results also indicate that the removal of RB5 by the developed UBC was stable at a wide range of pH. Two possible RB5 adsorption mechanisms on UBC, including electrostatic interaction and chemical reaction between RB5 and UBC, may be involved. The electrostatic interaction between the RB5 and UBC surface may explain the intensification of RB5 removal efficiency at pH 2. At a low pH, the prevailing positive charge of the UBC surface enhanced electrostatic attraction among anionic RB5 and the UBC surface, resulting in increased adsorption capacity [37]. The results were in accordance with the findings reported on adsorbents derived from sawdust and rice husk [41], coir pith [49], bamboo waste [37], and palm shell [50] for removing dye contaminants. Figure 7 shows that the isoelectric point of prepared UBC was at pH 2.20. At pH 2, the surface charge of UBC was positive; this supported the high RB5 removal. The removal efficiency in the pH range of 3 to 12 was lower than removal efficiency at pH 2, and its behavior and zeta-potential pattern (Figure 7) seemed to be in a good agreement. At alkaline pH, RB5 adsorption still occurred, suggesting the second process, such as chemisorption, might appear between pH 3 and 12, as seen in the additional peaks on FTIR spectrum of UBC-adsorbed RB5 [51]. It should be noted that although the best performance of UBC for RB5 removal was at pH 2, the operation under neutral conditions is more applicable for a real wastewater treatment system.

3.3.3. Initial RB5 Concentration

The pH of RB5 was adjusted to 2 based on the previous result in part 3.3.2. Figure 8 illustrates the initial concentration dependence of RB5 removal on the adsorbent. As the RB5 concentration increased, the removal efficiency gradually decreased, whereas the adsorption capacity increased. At higher RB5 concentration, a larger number of anions existed in the solution, which was easily dispersed and absorbed on UBC. Hence, the adsorption capacity became greater. A reversal of removal efficiency can be described by the adsorption sites on the UBC surface becoming filled upon increased adsorbate concentration, restricting the adsorption of the residual anions in the solution; consequently, the adsorption efficiency decreased. Therefore, the larger the initial concentration, the lower the removal efficiency. As seen in Figure 8, the highest adsorption capacity of 2.817

mg/g was obtained at an initial RB5 concentration of 60 mg/L. Hence, this optimal value was used for the next experiments.

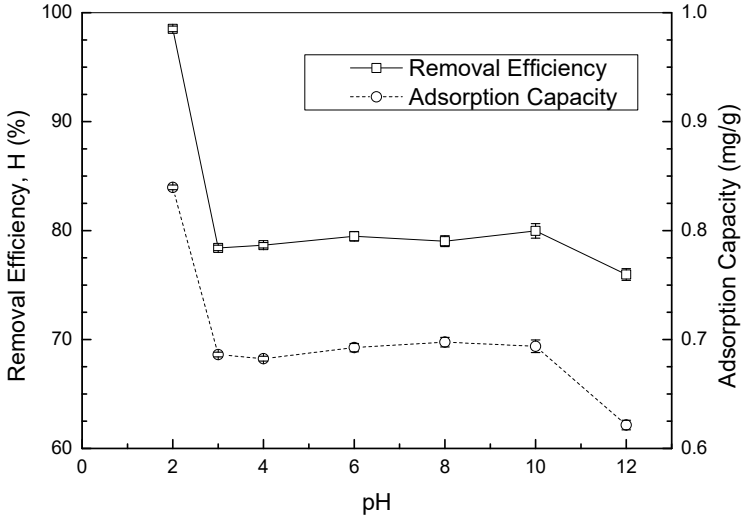

Figure 6. Impact of pH on adsorption of RB5 on UBC.

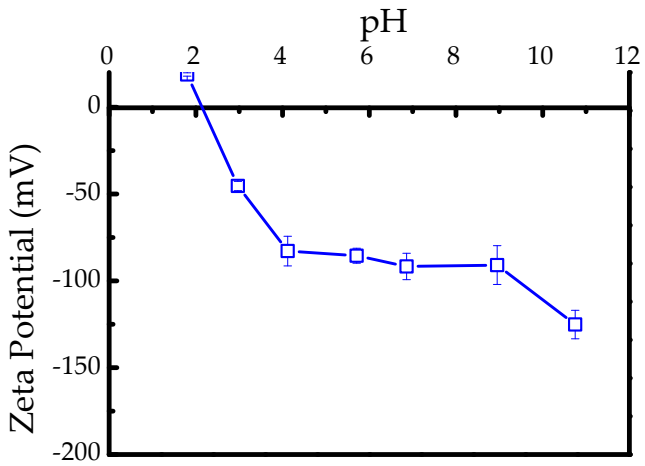

Figure 7. Zeta potential of UBC at different pH.

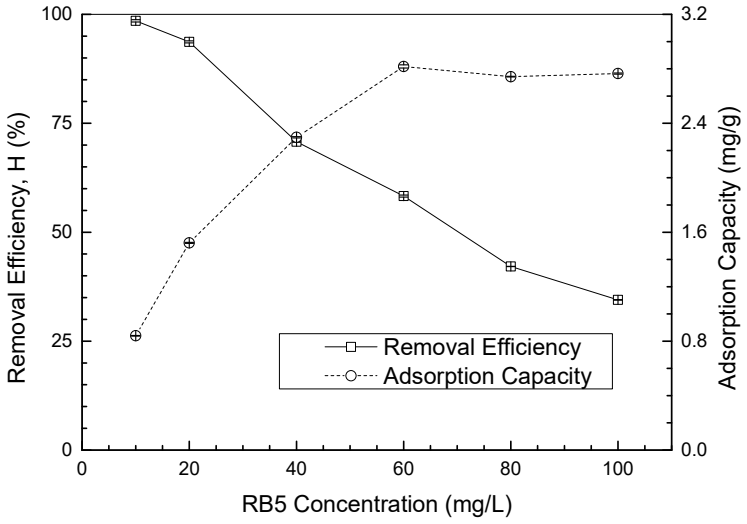

Figure 8. Impact of initial RB5 concentration on adsorption of RB5 on UBC.

3.3.4. Temperature and Reaction Time

Figure 9 illustrates the dependence of RB5 removal by UBC on experimental time at different temperatures of 15, 25, and 35 °C. Other empirical parameters were a UBC dosage of 10 g/L, pH 2, and an RB5 concentration of 60 mg/L. Since the temperature rose from 15 to 35 °C, the adsorption capacity enhanced from 3.223 to 3.486 mg/g, meaning that RB5 adsorption was endothermic [52]. This was in line with data reported previously at 18–38 °C [50] and 25–55 °C [28]. Besides, a similar result was obtained from the adsorption of methylene blue on banana peel biochar/iron oxide composite in which adsorption capacity enhanced from 500 mg/g at 20 °C to 750 mg/g at 40 °C at methylene-blue concentration of 25–500 mg/L and dosage of 0.5 g/L [53]. It was also stated that the penetration of adsorbate inside pores of UBC accelerated, and the creation of new active sites was more favorable in the condition of high temperature [28]. Simultaneously, the same experimental procedures were carried out at each reaction time and temperature employed for previous tests without UBC, and there was no RB5 removal observed (data not shown). It was also indicated that the adsorption capacity increased progressively with contact time and achieved a plateau region within 48 h. The adsorption process revealed a faster rate at the initial phase and a slight change at the latter phase. This was possibly explained by a decrease of available sites with time [54,55].

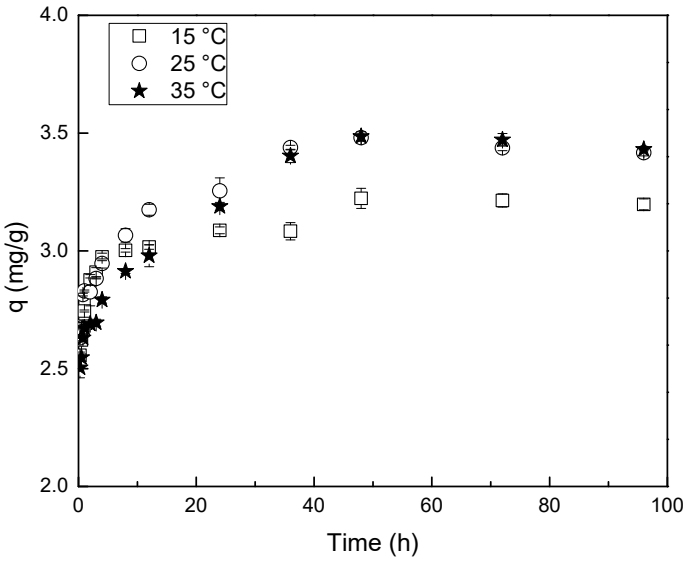

Figure 9. Impact of temperature and contact time on adsorption of RB5 on UBC.

3.4. Study on Adsorption Mechanism

3.4.1. Adsorption Isotherms

The plots of the linear form of Langmuir and Freundlich adsorption isotherms of RB5 on UBC are derived from the data of Section 3.3.3 for the reaction time of 3 h at 25 °C (Figure S3). The calculated isotherms parameters are displayed in Table 1. The R^2 value for the Langmuir isotherm model was high (0.999), indicating that it fit the adsorption data properly [56]. The adsorption of RB5 onto water bamboo-based UBC was regulated by monolayer adsorption, according to this discovery. The $1/n$ value obtained from the Freundlich isotherm model was less than one, suggesting that the adsorption mechanism followed normal Langmuir isotherm [57].

Table 1. Correlation coefficients and isotherm parameters for adsorption of RB5 on UBC.

Langmuir				Freundlich		
Q_m (mg/g)	Root-Mean-Square Deviation (RMSE)	b (L/mg)	R^2 (p-Value)	K_F(mg/g(L/mg)$^{1/n}$)	$1/n$	R^2 (p-Value)
2.811	2.814	0.362	0.999 (5.590×10^{-7}	1.134	0.202	0.964 (5.023×10^{-4})

3.4.2. Adsorption Kinetics

By comparing the kinetic data in Table 2 and Figure 10, it was ascertained that RB5 adsorption was described better by the pseudo-second-order kinetic model for all three different experiments. This confirmed that the adsorption of RB5 on UBC was mainly controlled by chemisorption. This data was in line with results from the RB5 adsorption on solid waste-based [37], palm shell-based [50], and chitosan-based [44] activated carbon. It also acted in good accordance with other dyes, such as Reactive Blue 19 [58] and Reactive Turquoise Blue QG [59]. The adsorption rate constant (k_2) increased from 0.007–0.105 with the temperature rising from 15–35 °C, which was likely to decrease solution viscosity.

Table 2. Pseudo-first- and pseudo-second-order kinetic parameters.

Temperature	1st Order		2nd Order	
	k_1	R^2 (p-Value)	k_2	R^2 (p-Value)
15 °C	0.072	0.704 (1.251×10^{-3})	0.007	1 $(< 2.2 \times 10^{-16})$
25 °C	0.061	0.946 (5.169×10^{-7})	0.055	0.998 (3.473×10^{-14})
35 °C	0.041	0.965 (7.592×10^{-8})	0.105	0.997 (7.218×10^{-13})

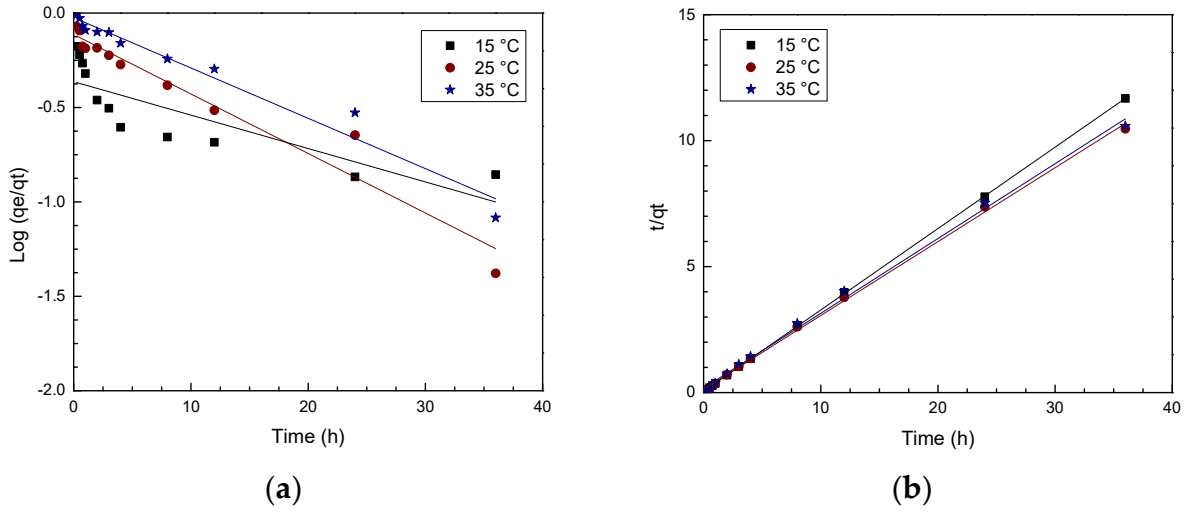

Figure 10. Adsorption kinetics for adsorption of RB5 on UBC (**a**) pseudo-first-order and (**b**) pseudo-second-order.

4. Conclusions

Water bamboo-derived BC was prepared by pyrolysis at 600 °C, and UBC was prepared to utilize pyrolysis accompanied by ultrasonic irradiation. Ultrasound successfully activated water bamboo-based carbon material with the efficient modifying of surface morphology and enhancement of surface area, leading to the higher adsorption rate of RB5 on UBC. The surface area and pore volume increased from 56.296 to 141.213 m^2/g and 0.013 to 0.039 cm^3/g. At pH 2, the RB5 concentration of 60 mg/L, UBC dosage of 10 g/L, solution temperature of 35 °C, and contact time of 48 h, UBC performed the highest adsorption capacity of 3.486 mg/g. However, the operation under neutral conditions and ambient temperature is more applicable for a real wastewater treatment system. Additionally, a pilot scale system test is necessary to obtain feasible operating parameters and investment costs for the practical application in the future. The mechanism of RB5 adsorption on UBC was found to follow the Langmuir adsorption isotherm with correlation coefficient R^2 = 0.999, indicating the monolayer type of adsorption. The adsorption kinetic is inclined towards pseudo-second-order kinetic, which described the chemisorption of RB5 on UBC. At pH 2, the prevailing positive charge of the UBC surface enhanced electrostatic attraction among anionic RB5 and the UBC surface. Chemisorption dominated the RB5 removal by UBC at pH 3 to 12. The carbon material modification using ultrasonic cavitation from

active bubbles at ambient temperature and a short time requirement within several minutes requires no additional chemicals and generates no harmful by-products. In this study, the results demonstrated that low-energy ultrasonic irradiation successfully activated the meso-surface area and porosity of carbon material, leading to the greater RB5 adsorption capacity of UBC with a higher reaction rate compared to that of BC. Therefore, ultrasonic irradiation is an applicable, green, energy-saving, and promising method to modify biochar from agricultural wastes for environmental remediation and agricultural productions.

Supplementary Materials: The following are available online at https://www.mdpi.com/article/10.3390/w13121615/s1, Figure S1: The structural formula of RB5, Figure S2: UV-Vis absorption spectra of RB5 at (a) pH 2, (b) pH 6, and (c) pH 10, Figure S3: Adsorption isotherms for adsorption of RB5 on UBC (a) Langmuir and (b) Freundlich.

Author Contributions: Conceptualization, T.T.N., T.H.T., K.-F.C. and Y.-P.T.; methodology, T.T.N., Y.-C.C. and K.-F.C.; investigation, T.T.N. and H.-H.C.; data curation, T.T.N., C.-K.T. and K.-F.C.; writing, review, and editing, T.T.N., K.-F.C., Y.-P.T., T.H.T. and C.-K.T.; Funding acquisition, K.-F.C. and Y.-P.T.; supervision, K.-F.C. All authors have read and agreed to the published version of the manuscript.

Funding: This work was financially supported by the Ministry of Education (MOE), Taiwan under the Cooperation and Exchange Program- ASEAN and South Asian Countries and the Ministry of Science and Technology (MOST), Taiwan with the grant number of 109-2321-B-260-001. Part of the experiments were completed with the support of the MOST with the grant number of 109-2927-I-224-001.

Institutional Review Board Statement: Not applicable.

Informed Consent Statement: Not applicable.

Data Availability Statement: Not applicable.

Acknowledgments: The authors are grateful to the MOE, Taiwan, for supporting the cooperation and exchange program between National Chi Nan University (NCNU), Taiwan, and University of Science, VNUHCM, Vietnam. Thanh Tam Nguyen obtained the opportunity for a research stay at NCNU with the financial support of this program. We also thank the MOST, Taiwan, for providing major equipment and part of the expense for the experiments of this collaborative research. Additional thanks are extended to the personnel at NCNU, Taiwan, and University of Science, VNUHCMC, Vietnam, and graduate students at NCNU, Taiwan for their assistance throughout this project.

Conflicts of Interest: The authors declare no conflict of interest.

References

1. Cederlund, H.; Börjesson, E.; Stenström, J. Effects of a wood-based biochar on the leaching of pesticides chlorpyrifos, diuron, glyphosate and MCPA. *J. Environ. Manag.* **2017**, *191*, 28–34. [CrossRef] [PubMed]
2. Doan, T.T.; Henry-Des-Tureaux, T.; Rumpel, C.; Janeau, J.L.; Jouquet, P. Impact of compost, vermicompost and biochar on soil fertility, maize yield and soil erosion in Northern Vietnam: A three year mesocosm experiment. *Sci. Total Environ.* **2015**, *514*, 147–154. [CrossRef] [PubMed]
3. Gámiz, B.; Velarde, P.; Spokas, K.A.; Hermosín, M.C.; Cox, L. Biochar soil additions affect herbicide fate: Importance of application timing and feedstock species. *J. Agric. Food Chem.* **2017**, *65*, 3109–3117. [CrossRef] [PubMed]
4. Streubel, J.D.; Collins, H.P.; Garcia-Perez, M.; Tarara, J.; Granatstein, D.; Kruger, C.E. Influence of contrasting biochar types on five soils at increasing rates of application. *Soil Sci. Soc. Am. J.* **2011**, *75*, 1402–1413. [CrossRef]
5. Yousaf, B.; Liu, G.; Wang, R.; Abbas, Q.; Imtiaz, M.; Liu, R. Investigating the biochar effects on C-mineralization and sequestration of carbon in soil compared with conventional amendments using the stable isotope (δ13C) approach. *GCB Bioenergy* **2017**, *9*, 1085–1099. [CrossRef]
6. Case, S.D.C.; McNamara, N.P.; Reay, D.S.; Stott, A.W.; Grant, H.K.; Whitaker, J. Biochar suppresses N_2O emissions while maintaining N availability in a sandy loam soil. *Soil Biol. Biochem.* **2015**, *81*, 178–185. [CrossRef]
7. Cayuela, M.L.; Jeffery, S.; van Zwieten, L. The molar H: Corg ratio of biochar is a key factor in mitigating N_2O emissions from soil. *Agric. Ecosyst. Environ.* **2015**, *202*, 135–138. [CrossRef]
8. Sheng, Y.; Zhu, L. Biochar alters microbial community and carbon sequestration potential across different soil pH. *Sci. Total Environ.* **2018**, *622–623*, 1391–1399. [CrossRef]
9. Smith, P. Soil carbon sequestration and biochar as negative emission technologies. *Glob. Chang. Biol.* **2016**, *22*, 1315–1324. [CrossRef]

10. Dehkhoda, A.M.; West, A.H.; Ellis, N. Biochar based solid acid catalyst for biodiesel production. *Appl. Catal. A Gen.* **2010**, *382*, 197–204. [CrossRef]
11. Dong, T.; Gao, D.; Miao, C.; Yu, X.; Degan, C.; Garcia-Pérez, M.; Rasco, B.; Sablani, S.S.; Chen, S. Two-step microalgal biodiesel production using acidic catalyst generated from pyrolysis-derived biochar. *Energy Convers. Manag.* **2015**, *105*, 1389–1396. [CrossRef]
12. Fang, G.; Liu, C.; Gao, J.; Dionysiou, D.D.; Zhou, D. Manipulation of persistent free radicals in biochar to activate persulfate for contaminant degradation. *Environ. Sci. Technol.* **2015**, *49*, 5645–5653. [CrossRef] [PubMed]
13. Ferreira, P.A.; Backes, R.C.; Martins, A.; De Carvalho, C.T.; Da Silva, R.A.B. Biochar: A low-cost electrode modifier for electrocatalytic, sensitive and selective detection of similar organic compounds. *Electroanalysis* **2018**, *30*, 2233–2236. [CrossRef]
14. Basri, N.H.; Deraman, M.; Kanwal, S.; Talib, I.A.; Manjunatha, J.G.; Aziz, A.A.; Farma, R. Supercapacitors using binderless composite monolith electrodes from carbon nanotubes and pre-carbonized biomass residues. *Biomass Bioenergy* **2013**, *59*, 370–379. [CrossRef]
15. Farma, R.; Deraman, M.; Awitdrus, A.; Talib, I.A.; Taer, E.; Basri, N.H.; Manjunatha, J.G.; Ishak, M.M.; Dollah, B.N.M.; Hashmi, S.A. Preparation of highly porous binderless activated carbon electrodes from fibres of oil palm empty fruit bunches for application in supercapacitors. *Bioresour. Technol.* **2013**, *132*, 254–261. [CrossRef] [PubMed]
16. Goodman, P.A.; Li, H.; Gao, Y.; Lu, Y.F.; Stenger-Smith, J.D.; Redepenning, J. Preparation and characterization of high surface area, high porosity carbon monoliths from pyrolyzed bovine bone and their performance as supercapacitor electrodes. *Carbon N. Y.* **2013**, *55*, 291–298. [CrossRef]
17. Tang, L.; Yu, J.; Pang, Y.; Zeng, G.; Deng, Y.; Wang, J.; Ren, X.; Ye, S.; Peng, B.; Feng, H. Sustainable efficient adsorbent: Alkali-acid modified magnetic biochar derived from sewage sludge for aqueous organic contaminant removal. *Chem. Eng. J.* **2018**, *336*, 160–169. [CrossRef]
18. Zhang, K.; Sun, P.; Zhang, Y. Decontamination of Cr(VI) facilitated formation of persistent free radicals on rice husk derived biochar. *Front. Environ. Sci. Eng.* **2019**, *13*, 22. [CrossRef]
19. Reguyal, F.; Sarmah, A.K.; Gao, W. Synthesis of magnetic biochar from pine sawdust via oxidative hydrolysis of $FeCl_2$ for the removal sulfamethoxazole from aqueous solution. *J. Hazard. Mater.* **2017**, *321*, 868–878. [CrossRef]
20. Chatterjee, R.; Sajjadi, B.; Mattern, D.L.; Chen, W.Y.; Zubatiuk, T.; Leszczynska, D.; Leszczynski, J.; Egiebor, N.O.; Hammer, N. Ultrasound cavitation intensified amine functionalization: A feasible strategy for enhancing CO_2 capture capacity of biochar. *Fuel* **2018**, *225*, 287–298. [CrossRef]
21. Li, H.; Dong, X.; Da Silva, E.B.; de Oliveira, L.M.; Chen, Y.; Ma, L.Q. Mechanisms of metal sorption by biochars: Biochar characteristics and modifications. *Chemosphere* **2017**, *178*, 466–478. [CrossRef]
22. Wang, J.; Wang, S. Preparation, modification and environmental application of biochar: A review. *J. Clean. Prod.* **2019**, *227*, 1002–1022. [CrossRef]
23. Wang, C.; Wang, H.; Cao, Y. Pb(II) sorption by biochar derived from Cinnamomum camphora and its improvement with ultrasound-assisted alkali activation. *Colloids Surf. A Physicochem. Eng. Asp.* **2018**, *556*, 177–184. [CrossRef]
24. Shrestha, R. Ultrasound-Assisted Post-Pyrolysis Magnetization of Microporous Ultrasound-Assisted Post-Pyrolysis Magnetization of Microporous Biochar for Effective Removal of Heavy Metals Biochar for Effective Removal of Heavy Metals. Undergraduate Thesis, The University of Mississippi, University, MS, USA, 2020. Available online: https://egrove.olemiss.edu/hon_thesis (accessed on 15 June 2020).
25. Chatterjee, R.; Sajjadi, B.; Chen, W.Y.; Mattern, D.L.; Egiebor, N.O.; Hammer, N.; Raman, V. Low frequency ultrasound enhanced dual amination of biochar: A nitrogen-enriched sorbent for CO_2 Capture. *Energy Fuels* **2019**, *33*, 2366–2380. [CrossRef]
26. Sajjadi, B.; Chen, W.Y.; Adeniyi, A.; Mattern, D.L.; Mobley, J.; Huang, C.P.; Fan, R. Variables governing the initial stages of the synergisms of ultrasonic treatment of biochar in water with dissolved CO_2. *Fuel* **2019**, *235*, 1131–1145. [CrossRef]
27. Ahmad, A.A.; Hameed, B.H. Fixed-bed adsorption of reactive azo dye onto granular activated carbon prepared from waste. *J. Hazard. Mater.* **2010**, *175*, 298–303. [CrossRef] [PubMed]
28. Al-Degs, Y.S.; El-Barghouthi, M.I.; El-Sheikh, A.H.; Walker, G.M. Effect of solution pH, ionic strength, and temperature on adsorption behavior of reactive dyes on activated carbon. *Dyes Pigments* **2008**, *77*, 16–23. [CrossRef]
29. Sathian, S.; Rajasimman, M.; Radha, G.; Shanmugapriya, V.; Karthikeyan, C. Performance of SBR for the treatment of textile dye wastewater: Optimization and kinetic studies. *Alex. Eng. J.* **2014**, *53*, 417–426. [CrossRef]
30. Padmesh, T.V.N.; Vijayaraghavan, K.; Sekaran, G.; Velan, M. Biosorption of Acid Blue 15 using fresh water macroalga Azolla filiculoides: Batch and column studies. *Dyes Pigments* **2006**, *71*, 77–82. [CrossRef]
31. Heibati, B.; Rodriguez-Couto, S.; Amrane, A.; Rafatullah, M.; Hawari, A.; Al-Ghouti, M.A. Uptake of Reactive Black 5 by pumice and walnut activated carbon: Chemistry and adsorption mechanisms. *J. Ind. Eng. Chem.* **2014**, *20*, 2939–2947. [CrossRef]
32. Güzel, F.; Sayılı, H.; Sayılı, G.A.; Koyuncu, F. New low-cost nanoporous carbonaceous adsorbent developed from carob (Ceratonia siliqua) processing industry waste for the adsorption of anionic textile dye: Characterization, equilibrium and kinetic modeling. *J. Mol. Liq.* **2015**, *206*, 244–255. [CrossRef]
33. Shih, Y.F. Mechanical and thermal properties of waste water bamboo husk fiber reinforced epoxy composites. *Mater. Sci. Eng. A* **2007**, *445–446*, 289–295. [CrossRef]
34. Greluk, M.; Hubicki, Z. Kinetics, isotherm and thermodynamic studies of Reactive Black 5 removal by acid acrylic resins. *Chem. Eng. J.* **2010**, *162*, 919–926. [CrossRef]

35. Barrer, R.M. Expanded clay minerals: A major class of molecular sieves. *J. Incl. Phenom.* **1986**, *4*, 109–119. [CrossRef]
36. Inglezakis, V.J.; Loizidou, M.D.; Grigoropoulou, H.P. Equilibrium and kinetic ion exchange studies of Pb^{2+}, Cr^{3+}, Fe^{3+} and Cu^{2+} on natural clinoptilolite. *Water Res.* **2002**, *36*, 2784–2792. [CrossRef]
37. Ahmad, A.A.; Idris, A.; Hameed, B.H. Organic dye adsorption on activated carbon derived from solid waste. *Desalin. Water Treat.* **2013**, *51*, 2554–2563. [CrossRef]
38. Nguyen, T.T.; Asakura, Y.; Koda, S.; Yasuda, K. Dependence of cavitation, chemical effect, and mechanical effect thresholds on ultrasonic frequency. *Ultrason. Sonochem.* **2017**, *39*, 301–306. [CrossRef] [PubMed]
39. Yasuda, K.; Nguyen, T.T.; Asakura, Y. Measurement of distribution of broadband noise and sound pressures in sonochemical reactor. *Ultrason. Sonochem.* **2018**, *43*, 23–28. [CrossRef]
40. Yasuda, K. Sonochemical green technology using active bubbles: Degradation of organic substances in water. *Curr. Opin. Green Sustain. Chem.* **2021**, *27*, 100411. [CrossRef]
41. Ip, A.W.M.; Barford, J.P.; McKay, G. A comparative study on the kinetics and mechanisms of removal of Reactive Black 5 by adsorption onto activated carbons and bone char. *Chem. Eng. J.* **2010**, *157*, 434–442. [CrossRef]
42. Peter, A.; Chabot, B.; Loranger, E. Enhancing surface properties of softwood biochar by ultrasound assisted slow pyrolysis. In Proceedings of the 2019 IEEE International Ultrasonics Symposium (IUS), Glasgow, UK, 6–9 October 2019; pp. 2477–2480. [CrossRef]
43. Cardoso, N.F.; Pinto, R.B.; Lima, E.C.; Calvete, T.; Amavisca, C.V.; Royer, B.; Cunha, M.L.; Fernandes, T.H.; Pinto, I.S. Removal of remazol black B textile dye from aqueous solution by adsorption. *Desalination* **2011**, *269*, 92–103. [CrossRef]
44. Vakili, M.; Zwain, H.M.; Mojiri, A.; Wang, W.; Gholami, F.; Gholami, Z.; Giwa, A.S.; Wang, B.; Cagnetta, G.; Salamatinia, B. Effective adsorption of reactive black 5 onto hybrid hexadecylamine impregnated chitosan-powdered activated carbon beads. *Water* **2020**, *12*, 2242. [CrossRef]
45. Zhang, P.; Lo, I.; O'Connor, D.; Pehkonen, S.; Cheng, H.; Hou, D. High efficiency removal of methylene blue using SDS surface-modified ZnFe2O4 nanoparticles. *J. Colloid Interface Sci.* **2017**, *508*, 39–48. [CrossRef]
46. Santhosh, C.; Daneshvar, E.; Kollu, P.; Peräniemi, S.; Grace, A.N.; Bhatnagar, A. Magnetic SiO_2@$CoFe_2O_4$ nanoparticles decorated on graphene oxide as efficient adsorbents for the removal of anionic pollutants from water. *Chem. Eng. J.* **2017**, *322*, 472–487. [CrossRef]
47. Banerjee, S.; Chattopadhyaya, M.C. Adsorption characteristics for the removal of a toxic dye, tartrazine from aqueous solutions by a low cost agricultural by-product. *Arab. J. Chem.* **2017**, *10*, S1629–S1638. [CrossRef]
48. Subramaniam, R.; Kumar Ponnusamy, S. Novel adsorbent from agricultural waste (cashew NUT shell) for methylene blue dye removal: Optimization by response surface methodology. *Water Resour. Ind.* **2015**, *11*, 64–70. [CrossRef]
49. Santhy, K.; Selvapathy, P. Removal of reactive dyes from wastewater by adsorption on coir pith activated carbon. *Bioresour. Technol.* **2006**, *97*, 1329–1336. [CrossRef] [PubMed]
50. Mook, W.T.; Aroua, M.K.; Szlachta, M. Palm shell-based activated carbon for removing reactive black 5 dye: Equilibrium and kinetics studies. *BioResources* **2016**, *11*, 1432–1447. [CrossRef]
51. Malik, P.K. Use of activated carbons prepared from sawdust and rice-husk for adsoprtion of acid dyes: A case study of acid yellow 36. *Dyes Pigments* **2003**, *56*, 239–249. [CrossRef]
52. Hsueh, C.L.; Lu, Y.W.; Hung, C.C.; Huang, Y.H.; Chen, C.Y. Adsorption kinetic, thermodynamic and desorption studies of C.I. Reactive Black 5 on a novel photoassisted Fenton catalyst. *Dyes Pigments* **2007**, *75*, 130–135. [CrossRef]
53. Zhang, P.; O'Connor, D.; Wang, Y.; Jiang, L.; Xia, T.; Wang, L.; Tsang, D.C.; Ok, Y.S.; Hou, D. A green biochar/iron oxide composite for methylene blue removal. *J. Hazard. Mater.* **2020**, *384*, 121286. [CrossRef] [PubMed]
54. Ai, L.; Zhang, C.; Liao, F.; Wang, Y.; Li, M.; Meng, L.; Jiang, J. Removal of methylene blue from aqueous solution with magnetite loaded multi-wall carbon nanotube: Kinetic, isotherm and mechanism analysis. *J. Hazard. Mater.* **2011**, *198*, 282–290. [CrossRef] [PubMed]
55. Kim, H.; Watthanaphanit, A.; Saito, N. Simple Solution Plasma Synthesis of Hierarchical Nanoporous MnO_2 for Organic Dye Removal. *ACS Sustain. Chem. Eng.* **2017**, *5*, 5842–5851. [CrossRef]
56. Katsumi, T. Soil excavation and reclamation in civil engineering: Environmental aspects. *Soil Sci. Plant. Nutr.* **2015**, *61*, 22–29. [CrossRef]
57. Fytianos, K.; Voudrias, E.; Kokkalis, E. Sorption-desorption behaviour of 2,4-dichlorophenol by marine sediments. *Chemosphere* **2000**, *40*, 3–6. [CrossRef]
58. Isah, U.A.; Abdulraheem, G.; Bala, S.; Muhammad, S.; Abdullahi, M. Kinetics, equilibrium and thermodynamics studies of C.I. Reactive Blue 19 dye adsorption on coconut shell based activated carbon. *Int. Biodeterior. Biodegrad.* **2015**, *102*, 265–273. [CrossRef]
59. Schimmel, D.; Fagnani, K.C.; Dos Santos, J.B.O.; Barros, M.A.S.D.; Da Silva, E.A. Adsorption of turquoise blue qg reactive dye on commercial activated carbon in batch reactor: Kinetic and equilibrium studies. *Braz. J. Chem. Eng.* **2010**, *27*, 289–298. [CrossRef]